Plasma Size Scaling of Avalanche-like Heat Transport in Tokamaks

S. Jolliet 1), Y. Idomura 1)

1) Japan Atomic Energy Agency, Higashi-Ueno 6-9-3, Taitou, 110-0015 Tokyo

E-mail contact of main author: jolliet.sebastien@jaea.go.jp

Abstract. The influence of plasma size on global Ion Temperature Gradient turbulence is studied with the full-f Eulerian code GT5D [Idomura et al., Nucl. Fusion 49, 065029]. The gyrokinetic model includes a consistent neoclassical electric field as well as a fixed-power source operator, enabling long-time simulations with self-consistent turbulent transport and equilibrium profiles. The effects of plasma size (from $\rho^* = 1/100$ to $\rho^* = 1/225$) are studied by scaling the minor radius a and the input power. For the first time, worse-than-Bohm scaling is observed in experimentally realistic conditions. Using a random walk approach, the correlation length and time on the contrary suggest gyro-Bohm scaling. Global effects are investigated by looking at the force balance relation and the avalanches dynamics. It is found that the parallel momentum and radial electric field profiles are coupled. A low shearing rate region is induced in the large plasma size simulation and enhances heat transport. In this region, the dynamics of avalanches is altered. GT5D simulations therefore highlight avalanches as a non-local mechanism for broken gyro-Bohm scaling and point out the importance of the yet unknown plasma size effects on momentum transport.

1 Introduction

Plasma turbulence will play a crucial role in the performance of future fusion devices such as ITER, whose physical size $(\rho^*)^{-1}$ will be 2 to 3 times larger than existing Tokamaks, where $\rho^* = \rho_s/a$ is the relative gyroradius, ρ_s is the ion sound gyroradius and a is the minor radius of the Tokamaks. Heat, momentum and density transport coefficients need to be extrapolated from present days experiments. Heat transport is measured with the ion heat diffusivity $\chi = \chi_B(\rho^*)^{x_\rho}$, where $\chi_B = cT_e/eB$ is the the Bohm normalization. The transport can be characterized according to the exponent x_ρ. If $x_\rho = 1$, the scaling is gyro-Bohm like and will decrease with increasing plasma size. $x_\rho = 0$ is the Bohm-like scaling, for which transport is independent of the plasma size. $x_\rho < 0$ is the worse-than-Bohm scaling. In that case transport increases with plasma size. Extrapolation will be meaningful only if the physical processes do not change while ρ^* is decreased. In that respect, determining the behavior of plasma turbulence with plasma size is crucial.
Experiments on the DIII-D Tokamak showed that the electron heat transport scales gyro-Bohm like while ion heat transport scales Bohm-like or worse-than-Bohm-like in L-mode plasmas [1]: the overall scaling depends on the dominant transport channel. At present there is no clear explanation of broken gyro-Bohm scaling. Several mechanisms have been proposed, such as sheared flows stabilization [2] or turbulence spreading [3]. The ρ^* transition value as well as the flux-tube limit $\rho^* \to 0$ heat transport differed between Particle-In-Cell [4] and Eulerian calculations [5]. These discrepancies have been solved recently in Ref. [6], in which global Eulerian and PIC methods quantitatively agree provided a consistent magnetic equilibrium model is used.
A common feature of all previous gyrokinetic studies is the fixed-gradient model: global simulations experience profile relaxation which drives the system towards the marginality

state. This is avoided by adding an empirical source term which dynamically introduces some energy in the system in order to keep a nearly-fixed temperature gradient. Although such models are convenient from a theoretical point of view, they often have difficulties in simulating experiments, in which the total power input is fixed and the profiles are free to evolve. Recently, more realistic fixed-flux (or equivalently fixed-power) global gyrokinetic models have been developed [7]. Fixed-flux simulations reach a steady-state in which the temperature profile is close to the marginal stability. Since ITER will operate close to the critical gradient, it is necessary to re-examine the plasma size scaling with realistic fixed-flux gyrokinetic simulations. In this paper, this topic will be addressed with the global Eulerian gyrokinetic code GT5D [7].
The rest of the paper is organized as follows. The GT5D code is described in Sec. 2. Results on the ρ^* scaling are exposed in Sec. 3. Finally, conclusions are exposed in Sec. 4.

2 The GT5D code

The detailed implementation of the GT5D code can be found in Refs. [7] and [8]. It is briefly summarized for completeness.
GT5D is a five-dimensional full-f Vlasov code which solves a gyrokinetic equation in Tokamaks:

$$\frac{\partial \mathcal{J}}{\partial t} + \nabla \cdot (\mathcal{J}\dot{\mathbf{R}} f) + \frac{\partial}{\partial v_\parallel}(\mathcal{J}\dot{v}_\parallel f) = \mathcal{J}\Big[C(f) + S_{\rm src}(f) + S_{\rm snk}(f)\Big] \tag{1}$$

where $f(\mathbf{R}, v_\parallel, \mu, t)$ is the ion guiding-center distribution function, $\mathbf{R}$ is the guiding-center position, $v_\parallel$ is the velocity parallel to the magnetic field, μ is the magnetic moment and $\mathcal{J}$ is the phase-space Jacobian. The nonlinear equations of motion $(\dot{\mathbf{R}}, \dot{v}_\parallel)$ are obtained from a Hamiltonian approach $\dot{\mathbf{R}} \equiv \{\mathbf{R}, H\}$ and $\dot{v}_\parallel \equiv \{v_\parallel, H\}$, where $\{F, G\}$ is the Poisson bracket operator and H is the Hamiltonian [8]. The Vlasov equation is solved on a $(N_R, N_Z, N_\varphi, N_{v_\parallel}, N_\mu)$ grid, where (R, Z, φ) are cylindrical coordinates.
The collision operator $C(f)$ is a linearized, drift-kinetic Fokker-Planck operator $C(f) \equiv C_T(\delta f) + C_F(f)$, where $C_T(\delta f)$ is the test-particle operator and $C_F(f)$ is the field-particle operator. In particular, the field-particle operator is constructed numerically in order to conserve density, parallel momentum and energy up to machine precision. Finite Larmor Radius (FLR) effects in the collision operator are neglected.
The source operator is $S_{\rm src} = A_{\rm src}(\mathbf{R})\tau_{\rm src}^{-1}(f_{M1} - f_{M2})$, where $A_{\rm src}$ is a deposition profile, f_{M1} and f_{M2} are (shifted) Maxwellian distributions and τ_{src} is a time constant. τ_{src} is set by imposing zero particle and momentum input, but fixed power input $P_{\rm in}$:

$$0 = \int S_{\rm src} {\rm d}^6 Z = \int m_i v_\parallel S_{\rm src} {\rm d}^6 Z \tag{2}$$

$$P_{\rm in} = \int \Big(\frac{1}{2} m_i v_\parallel^2 + \mu B\Big) S_{\rm src} {\rm d}^6 Z \tag{3}$$

where ${\rm d}^6 Z$ is the phase space volume. The sink operator is $S_{\rm snk} = A_{\rm snk}(\mathbf{R})\tau_{\rm snk}^{-1}(f_0 - f)$, where $A_{\rm snk}$ is a deposition profile, f_0 is the initial distribution and $\tau_{\rm snk}$ is a time constant. The source profile $A_{\rm src}$ extends from $r/a = 0$ to $r/a = 0.5$ and the sink profile extends from $r/a = 0.9$ to $r/a = 1.0$. The $0.5 < r/a < 0.9$ is the source free region.
The self-consistency is imposed by the quasi-neutrality equation:

$$-\nabla_\perp \cdot \frac{\rho_{ti}^2}{\lambda_{Di}^2}\nabla_\perp \phi + \frac{1}{\lambda_{De}^2}\Big(\phi - \langle\phi\rangle_f\Big) = 4\pi e\Big[\int f\delta(\mathbf{R} + \rho - \mathbf{x}){\rm d}^6 Z - n_{0e}\Big] \tag{4}$$

where $\mathbf{R}+\rho$ is the particle position, ρ_{ti} is the Larmor radius evaluated with the thermal velocity v_{ti}, $\lambda_{Di}, \lambda_{De}$ are the ion and electron Debye lengths, $\langle\cdot\rangle_f$ is a flux-surface-average operator and n_{0e} is the equilibrium electron density. Electrons are adiabatic. Dirichlet boundary conditions are imposed at the plasma edge, while a free boundary is imposed at the magnetic axis. The quasi-neutrality equation is solved using quadratic B-splines finite elements on a 2D grid (N_r, N_χ) where r is the radial coordinate and χ is the straight-field-line angle. A Fourier filter [9] is applied to remove small parallel wavelengths. Such procedure does not influence the steady state of the simulations.

3 Plasma size scaling

GT5D simulations are characterized by steady-state profiles constrained by the Force Balance Equation (FBE):

$$\frac{m_i\Omega_i}{T_i I(\psi)}\frac{\mathrm{d}\psi}{\mathrm{d}r}V_\parallel(r) = \left[(k-1)\frac{\mathrm{dln}\,T_i}{\mathrm{d}r} - \frac{\mathrm{dln}\,n_i}{\mathrm{d}r} + \frac{e}{T_i}E_r\right] \tag{5}$$

where ψ is the poloidal flux, $I(\psi) = RB_\varphi$, n_i is the ion density, T_i is the ion temperature, $V_\parallel(r)$ is the flux-surface-averaged parallel velocity profile, E_r is the radial electric field and $k = k(\nu^*)$ is a coefficient of the neoclassical poloidal flow. In addition, the input power will fix, on time-average, the temperature profile. The latter is locally perturbed by avalanches propagating outwards or inwards depending on the sign of the electric field shear. The FBE indicates how to modify the radial electric field which regulates the heat transport level, for example by adding an external momentum source [10]. In r/a units, density and temperature profiles have similar shape regardless of plasma size, which means that $\mathrm{d}\ln T_i/\mathrm{d}r, \mathrm{d}\ln n_i/\mathrm{d}r \propto \rho_*$. For simulations without momentum input, one can assume that intrinsic momentum generation will be small, implying $E_r \propto \rho_*$. It is expected that increasing plasma size will reduce the electric field amplitude which will affect the shearing rate of turbulence, hence the heat transport level. The FBE also reveals the link between heat and momentum transport.

Standard CYCLONE simulations are presented. 1/6 wedge torus at $\rho^* = 1/150$ is simulated. The value of ρ^* is computed with the volume averaged profiles, and would be 10% larger if the value of profiles at the reference surface $r/a = 0.5$ were chosen. The initial temperature gradient is $R/L_{Ti} = 10$. The numerical parameters are $\Delta t = 5\Omega_i^{-1}$, $(N_R, N_Z, N_\varphi, N_{v_\parallel}, N_\mu) = (160, 160, 32, 80, 20)$ and $(N_r, N_\chi) = (128, 256)$ for the finite element grid. Only 16 toroidal modes are kept in the system and the others are filtered out. This ensures a minimum resolution of 4 points per wavelength to avoid aliasing effects. The input heating power is $P_{\mathrm{in}} = 2MW$. The heat deposition profile extends between $r/a = 0$ and $r/a = 0.5$, while the sink deposition profile extends from $r/a = 0.9$ to $r/a = 1.0$ with $\tau_{\mathrm{snk}}^{-1} = 0.1 v_{ti}/a$ (see [7]). Then, simulations at $\rho^* = 1/100$ and $\rho^* = 1/225$ are performed by scaling the minor radius a, the major radius R_0, the grid resolutions (N_R, N_Z, N_φ) and (N_r, N_χ) and the time step Δt proportionally to $1/\rho^*$. Thereby, the spatial resolution per Larmor radius and the time step in a/c_s units stay constant. The $\rho^* = 1/225$ simulation needed $1.7 \cdot 10^6$ CPU hours on the BX900 machine to run up to $5000 a/c_s$.

Note that modifying ρ^* in this way will also scale the effective collisionality ν_*. For $\rho^* = 1/100, 1/150, 1/225$, neoclassical transport is $36\%, 20\%$ and 13% of the turbulent transport in the source free region where the average ν^* in the source-free region is $\nu_* = 0.034, 0.050, 0.075$. Note that the combined effect of ρ^* and ν_* variation gives a

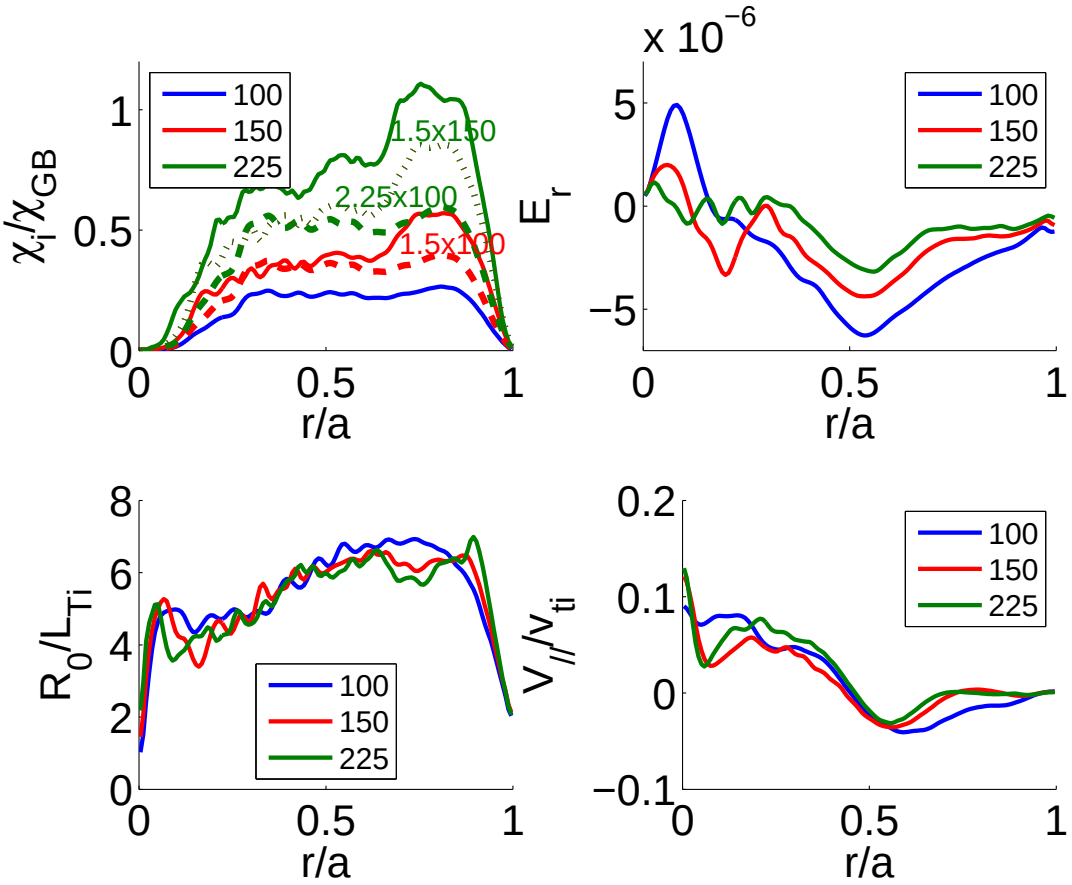

Figure 1: Radial profile of χ_i/χ_{GB} (top,left),R_0/L_{Ti} (bottom,left), E_r (top,right) and $V_{\|}/v_{ti}$ (bottom,right) for the $\rho^* = 1/100$ (blue), $\rho^* = 1/150$ (red) and $\rho^* = 1/225$ (green) simulations. All profiles are averaged between $t_1 = 1300a/c_s$ and $t_2 = 5130a/c_s$. The dashed curves are the Bohm-like scaled diffusivity from the $\rho^* = 1/100$ simulation. The dotted curve is the Bohm-like scaled diffusivity from the $\rho^* = 1/150$ simulation

roughly constant neoclassical transport $\chi_{\rm neo}/\chi_{GB} = 0.086, 0.093, 0.12$. The ν_* variation is therefore considered as small. Special care must be taken for the input power $P_{\rm in}$. Assuming a simple form $Q_i \cong P_{\rm in}/S$ for the heat flux with $S = 2\pi^2 R_0 r^2$ gives $\chi_i/\chi_{GB} \propto 1/\rho^*$ (Bohm scaling) if $P_{\rm in} \propto 1/\rho^*$ and R_0/L_{Ti} is fixed. ρ^* scaling experiments [11] also scale the input power with plasma size.

Fig. 1 shows the radial profile of the heat diffusivity averaged over 2.5 collision times at the end of the simulation. Compared to the $\rho^* = 1/100$ profile, the $\rho^* = 1/150$ one is Bohm-like up to $r/a = 0.6$ and then slightly worse-than-Bohm between $r/a = 0.6$ and $r/a = 0.8$. Then both profiles go to zero due to the sink operator which is active in $0.9 < r/a < 1.0$. However, the $\rho^* = 1/225$ profile scales worse-than-Bohm over the whole radius, especially between $r/a = 0.6$ and $r/a = 0.8$. From the average values of χ_i in $0.5 < r/a < 0.8$ region, the scaling is $\chi_i = \chi_B(\rho^*)^{-0.66}$ which is clearly worse-than-Bohm. The high transport near $r/a = 0.8$ creates a hollow structure in the temperature profile: the average values in the source-free region $0.5 < r/a < 0.8$ are $R/L_{Ti} = 6.7, 6.3, 6.1$ for $\rho_* = 1/100, 1/150, 1/225$, showing a dependence of the critical gradient on ρ_*. Worse-than-Bohm scaling has already been observed in experiments. On DIII-D, the ion diffusivity in L-mode plasmas scale like $\chi_i \propto \chi_B(\rho^*)^{-0.5\pm0.3}$ for two different heating methods, while

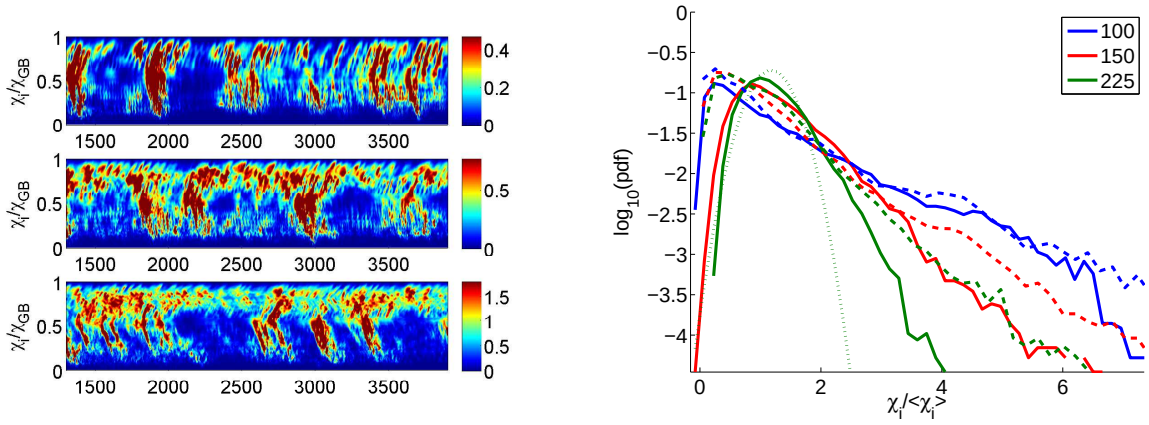

Figure 2: Left: radial and temporal evolution of χ_i/χ_{GB} for the $\rho^* = 1/100$ (top), $\rho^* = 1/150$ (middle) and $\rho^* = 1/225$ (bottom) simulations. The color axis upper value has been set to two times the average value (taken in the source-free region $0.5 < r/a < 0.8$ over the whole time interval). Right: probability distribution function of $\chi_i/\langle\chi_i\rangle$ for the $\rho^* = 1/100$ (blue), $\rho^* = 1/150$ (red) and $\rho^* = 1/225$ (green) simulations between $0.55 < r/a < 0.69$ (dashed line) and $0.7 < r/a < 0.85$ (solid line). The pdfs are constructed for $1300a/c_s < t < 5130a/c_s$. For each ρ^* value, $\langle\chi_i\rangle$ is χ_i averaged over $0.5 < r/a < 0.85$. The dotted curve is a Gaussian pdf with same average and variance as the $\rho^* = 1/225$ curve.

H-mode plasmas have a gyro-Bohm scaling $\chi_i \propto \chi_B \rho^*$ [1]. On JT-60U, a mass scan revealed that going from deuterium to hydrogen plasma, thus decreasing ρ^* by a factor $\sqrt{2}$, required 2 times more input power [12] to keep the same equilibrium profiles and stored energy. Although details about the diffusivity were not given, the scaling of the input power suggests worse-than-Bohm scaling. The ρ_* value for these experiments is estimated to vary from 1/350 to 1/500. Therefore, worse-than-Bohm scaling may occur in large plasma sizes as well. Several theoretical works have reported worse-than-Bohm scaling, however the requirements did not correspond to realistic Tokamak experiments. In Ref. [2], quasi-3D fixed-flux fluid simulations find worse-than-Bohm scaling for very small plasma size ($\rho^* > 1/100$) close to the marginality point. In Ref. [13], fixed-gradient GYRO simulations find worse-than-Bohm scaling for strong profile shearing cases. In experiments, such profiles could only exist inside Internal Transport Barriers. Those works emphasize the closeness to the marginal point as a necessary condition for worse-than-Bohm scaling, a common feature also in GT5D simulations, but this phenomenon was studied for experimentally infrequent parameters. However, GT5D simulations are the first to observe worse-than-Bohm scaling in experimentally relevant conditions. Note that for very stiff temperature profiles, a Bohm scaling could be trivially obtained from the Bohm scaling of the power input. A ρ^* scan has been performed at fixed power input, corresponding to a gyro-Bohm scaling of the power input: the heat diffusivity also has a worse-than-Bohm scaling.

Non local effects are investigated by looking at the avalanches structure. From Fig. 2, one sees that all 3 cases exhibit inward and outward avalanches depending on the sign of the electric field shear [7]. Large bursty events are more frequent for small plasma sizes. The avalanche speed is roughly $v_A = 0.5\rho^* c_s$, both inwards and outwards. The speed of avalanches seems approximatively constant throughout the plasma. Assuming $\chi_i \sim \Delta r^2/\Delta t$ and taking $\Delta r/\Delta t \sim v_A \sim 0.5\rho^* c_s$ and $\Delta r = a$ gives a Bohm scaling

$\chi_i/\chi_{GB} \sim (\rho^*)^{-1}$. Measurements of the correlation length and time of the $n \neq 0$ potential give $\Delta r = 4.4, 5.2, 5.9\rho_s$ and $\Delta t = 2.0, 2.4, 2.6a/c_s$ for $\rho^* = 1/100$, $1/150$, $1/225$ which would *a contrario* suggest gyro-Bohm scaling. Similar values were obtained in DIII-D experiments [14], although the power balance analysis revealed worse-than-Bohm scaling for similar experiments [1]. In experiments, one observes a mismatch between the heat diffusivities computed from the power balance relation and from a random walk estimate: non locality breaks down the assumption of diffusive transport. However, in the $\rho^* = 1/225$ case the dynamics of avalanches is altered in the $0.7 < r/a < 0.85$ region: there is no favored propagation direction, and both inward and outward avalanches coexist. The right plot of Fig. 2 shows the probability distribution function of the normalized ion heat diffusivity $\chi_i/ < \chi_i >$ in the region $0.55 < r/a < 0.69$ and in the region $0.7 < r/a < 0.85$. $\langle \chi_i \rangle$ is the averaged value in the $0.55 < r/a < 0.85$ value. All curves show non-diffusive transport. This feature is more pronounced for small plasma sizes. Then, one can see that the $\rho* = 1/100$ pdf remains essentially the same in both regions, while for $\rho^* = 1/150$ and $\rho^* = 1/225$ the $0.7 < r/a < 0.85$ region is more diffusive. The $\rho^* = 1/100$ case shows intermittent-like transport, while the $\rho^* = 1/225$ shows more frequent bursts in the flat shear region.

In order to explain the different features of avalanches, the time-averaged electric field profile is represented on Fig. 1. As explained above, the minimum of E_r is proportional to ρ^*. However, Fig. 1 reveals that for $\rho^* = 1/150$ and $\rho^* = 1/225$, a plateau is forming near the plasma edge, and the E_r profile no longer has a triangular shape. In the region $0.3 < r/a < 0.9$, three distinct zones appear, a negative shear region, a positive shear region and a flat shear region. From Fig. 1, one can see that the time-averaged parallel velocity profile has the same shape as the time-averaged electric field. In particular, $V_{//}(r)$ is flat in the region $0.7 < r/a < 0.85$ for $\rho^* = 1/150, 1/225$. Such relation is due to the force balance equation, Eq.(5). Consequently, the coupling between momentum and heat transport might be responsible for the local enhancement of χ_i/χ_{GB} observed in the $\rho^* = 1/225$ simulation. Plasma size effects on momentum transport are still largely unknown and are beyond the scope of this paper.

It is commonly accepted that suppression of turbulence happens when the shearing rate of the electric field γ_E exceeds the linear growth rate γ, where [15]:

$$\gamma_E = \left| \frac{cr}{q(r)B_0} \frac{\partial}{\partial r} \left(\frac{q(r)}{r} E_r \right) \right| \tag{6}$$

where $q(r)$ is the safety factor profile. A simple model [2] for broken gyro-Bohm scaling is to state that ITG turbulence is modified by profile and electric field shearing effects, $\gamma \cong \gamma_0 - \gamma^* - \gamma_E$, where γ_0 is the local growth rate and $\gamma^* a/c_s, \gamma_E a/c_s \propto \rho^*$ are the normalized profile and electric shearing rate. Such arguments lead to $\chi \sim \chi_B \rho^* (1 - \alpha^* \rho^*)$ where $1 - \alpha^* \rho^* = \gamma/\gamma_0$. Such diffusivity varies from worse-than-Bohm scaling to Gyro-Bohm scaling, but the transitions depend on α^*, which in turns depends on the plasma parameters.

In the present simulations, the instantaneous shearing rate $\gamma_E a/c_s$ approximatively scales like ρ^*, but it is rather the shearing rate of the time-averaged electric field which is efficient in suppressing turbulence [16]. The growth rates of the most unstable linear modes $k_\theta \rho_{Li} = 0.3$ for $\rho^* = 1/100, 1/150, 1/225$ and $R/L_{Ti} = 6.7.6.3, 6.1$ are $\gamma a/c_s = (0.073, 0.073, 0.074)$. In units, the shearing rates of the time-averaged profiles observed for $\rho^* = 1/100, 1/150, 1/225$ are $\gamma_E a/c_s = (0.084, 0.074, 0.80), (0.067, 0.070, 0.065)$ and $(0.048, 0.018, 0.010)$ in the negative, positive and flat regions, respectively. In the V-

shaped region, one has $\gamma_L \cong \gamma_E$ while in the flat region one has $\gamma_L > \gamma_E$. This is especially true for the $\rho^* = 1/150$ and $\rho^* = 1/225$ cases, where the heat transport is enhanced by 30% compared to the positive shear region. One remarks that in the V-shaped region, $\gamma_E a/c_s$ is almost constant, meaning that the $\gamma_E a/c_s \propto \rho^*$ assumption breaks down. Transport models assume $\gamma_E a/c_s \propto \rho^*$. GT5D simulations suggest that this hypothesis should be modified to reflect the effects of momentum transport.

4 Conclusions

Using a full-f Eulerian approach, the effects of plasma size on fixed-flux ITG turbulence with consistent equilibrium profiles close to the marginal stability have been studied for the first time. For plasma size ranging from $\rho^* = 1/100$ to $\rho^* = 1/225$, the heat diffusivity is found to scale like $\chi_i \propto \chi_B (\rho^*)^{-0.66}$: this is the first theoretical study who shows worse-than-Bohm scaling in experimentally realistic conditions. Turbulent correlation length and time are in good agreement with experimental measurements but the associated random walk estimate suggest gyro-Bohm scaling. For the largest plasma size simulated, $\rho^* = 1/225$, the dynamics of avalanches is changed depending on the radial electric field profile: through the force balance equation, a flat electric field region develops and increases the heat transport. The coupling between heat and momentum transport due to the force balance equation breaks down the usual assumption $\gamma_E a/c_s \propto \rho^*$. Consequently, the effects of momentum transport should be included in future heat transport models. To this aim, future work is needed to clarify the role of momentum transport, whose ρ^* effects are largely unknown yet. Another important issue is the transition point from Bohm to gyro-Bohm in fixed-flux simulations, which may depend on the closeness to the marginal point. Finally, it must be established if there is a link between the transition point and the avalanche dynamics. Simulations of larger plasma sizes are therefore required, which should be possible with the next generation of super-computers.

References

[1] PETTY, C. C., LUCE, T. C., BURRELL, K. H., et al., Phys. Plasmas **2** (1995) 2342.

[2] GARBET, X. and WALTZ, R. E., Phys. Plasmas **3** (1996) 1898.

[3] HAHM, T. S., DIAMOND, P. H., LIN, Z., ITOH, K., and ITOH, S.-I., Plasma Phys. Control. Fusion **46** (2004) A323.

[4] LIN, Z., ETHIER, S., HAHM, T., and TANG, W. M., Phys. Rev. Lett. **88** (2002) 195004.

[5] CANDY, J., WALTZ, R., and DORLAND, W., Phys. Plasmas **11** (2004) L25.

[6] MCMILLAN, B. F., LAPILLONNE, X., BRUNNER, S., et al., accepted for publication in Phys. Rev. Lett. (2010).

[7] IDOMURA, Y., URANO, H., AIBA, N., and TOKUDA, S., Nucl. Fusion **49** (2009) 065029.

[8] IDOMURA, Y., IDA, M., KANO, T., AIBA, N., and TOKUDA, S., Comp. Phys. Commun. **179** (2008) 391.

[9] MCMILLAN, B. F., JOLLIET, S., BOTTINO, A., et al., Comp. Phys. Commun. **181** (2010) 715.

[10] IDOMURA, Y., JOLLIET, S., YOSHIDA, M., and URANO, H., This conference .

[11] PETTY, C. C., LUCE, T. C., PINSKER, R. I., et al., Phys. Rev. Lett. **74** (1995) 1763.

[12] URANO, H., TAKIZUKA, T., KAMADA, Y., et al., Nucl. Fusion **045008** (2008) 045008.

[13] WALTZ, R., CANDY, J., and ROSENBLUTH, M. N., Phys. Plasmas **9** (2002) 1938.

[14] MCKEE, G. R., PETTY, C. C., WALTZ, R. E., et al., Nucl. Fusion **41** (2001) 1235.

[15] BURRELL, K. H., Phys. Plasmas **4** (1997) 1499.

[16] HAHM, T. S., BEER, M. A., LIN, Z., et al., Phys. Plasmas **6** (1999) 922.